Appl. Phys. B 75, 317–327 (2002)
DOI: 10.1007/s00340-002-0978-5

Applied Physics B
Lasers and Optics

The application of quasi-phase-matched parametric light sources to practical infrared chemical sensing systems

T.J. KULP[1,✉]
S.E. BISSON[1]
R.P. BAMBHA[1]
T.A. REICHARDT[1]
U.-B. GOERS[1,*]
K.W. ANIOLEK[1,*]
D.A.V. KLINER[1]
B.A. RICHMAN[1,**]
K.M. ARMSTRONG[1]
R. SOMMERS[1]
R. SCHMITT[1,***]
P.E. POWERS[2]
O. LEVI[3]
T. PINGUET[3]
M. FEJER[3]
J.P. KOPLOW[4]
L. GOLDBERG[4]
T.G. MCRAE[5]

[1] Sandia National Laboratories, Livermore, CA 94550-0969, USA
[2] Department of Physics, University of Dayton, Dayton, OH 45469-2314, USA
[3] E.L. Ginzton Laboratory, Stanford University, Stanford, CA 94305, USA
[4] Naval Research Laboratory, Washington, DC 20375-5672, USA
[5] Laser Imaging Systems, Punta Gorda, FL 33983, USA

Received: 15 April 2002/Revised version: 6 June 2002
Published online: 12 September 2002 •

ABSTRACT Quasi-phase-matched (QPM) materials allow the generation of spectroscopically useful infrared radiation in an efficient and broadly tunable format. Here, we describe several applications of QPM-based light sources to remote and local chemical sensing. The remote systems are gas imagers that employ a fiber-pumped continuous-wave optical parametric oscillator or a microlaser-pumped, diode-seeded optical parametric amplifier as the illumination source. Technology described for local sensing includes a cavity ring down spectrometer that employs a novel optical parametric generator–amplifier to achieve $\geq 350\,\mathrm{cm}^{-1}$ of contiguous tuning and a long-wave infrared light source based on QPM GaAs. In each case the use of QPM materials in conjunction with effective pump sources instills simplicity and ruggedness into the sensing systems.

PACS 42.65.Yj; 42.68.Wt; 82.80.Gk

1 Introduction

Following its emergence as a practical methodology, quasi-phase matching (QPM) [1] has been used to demonstrate performance in nonlinear conversion that was previously difficult or impossible to achieve. These advances have, in turn, offered new capabilities to fields that use lasers as tools. One such field is optical chemical sensing, where lasers excite spectral transitions in molecules for the purpose of quantifying or identifying chemical samples. These analyses can be performed either in the laboratory, within a sensor placed in the field, or at a distance using a remote probe (e.g. a lidar).

Here, we summarize some of our applications of QPM-based light sources to gas-phase chemical sensing measurements in the infrared (IR) spectral region. Detection at IR wavelengths is of particular interest because nearly all molecules absorb there at distinct frequencies that are indicative of their skeletal structure [2]. The link between structure and absorption exists because IR excitation causes a change in the rotational and vibrational (rovibrational) state of the molecule. The strongest absorptions are the fundamental absorptions, which accompany a change in vibrational quantum number of one for a particular mode and occur at wavelengths between ~ 2.5 and $20\,\mu\mathrm{m}$. Although this range is desirable for ultra-sensitive detection, many measurements [3] have been made at wavelengths shorter than $2.5\,\mu\mathrm{m}$ (in the so-called overtone region where weaker multiple quantum transitions occur), because of the lack of suitable lasers at long wavelengths.

The present state of the art in continuously tunable lasers suitable for chemical sensing in the mid- to long-wave IR includes diode lasers (lead-salt, quantum cascade, and others) and sources based on nonlinear conversion. While lead-salt diode lasers have been the workhorse of numerous successful measurements and sensing systems [4, 5], they exhibit shortcomings in power, beam quality, and spectral reproducibility that can affect performance. Quantum cascade lasers [6] (QCLs) hold great promise as an alternative that is free from some or all of these problems. QCLs have been shown to produce significant output power while maintaining single-longitudinal-mode operation and being reproducibly tunable in a manner suitable for spectroscopy [7]. To date, however, distributed-feedback (DFB) continuous-wave (cw) QCLs exhibit cw single-mode tuning over only a modest width ($\sim 10\,\mathrm{cm}^{-1}$) and generally require cryogenic cooling to achieve this performance (although room-temperature operation has recently been demonstrated in a buried het-

✉ Fax: +1-925/294-2595, E-mail: tjkulp@sandia.gov
*Present address: Corning Inc., Corning, NY 14831, USA
**Present address: Blue Leaf Networks, Sunnyvale, CA 94086, USA
***Present address: Sandia National Laboratories, Albuquerque, NM 87185, USA

erostructure laser [8]). Moreover, diode lasers are limited in the choice of output that they provide – for example IR diode lasers cannot produce the high-energy pulses that are required for use in a lidar.

Nonlinear conversion offers a versatile approach for IR generation due to the broadband nature of parametric gain, the wide variety of temporal formats in which light may be produced, and the ability to operate free from cryogenic liquids. In general, $\chi^{(2)}$ interactions are used to couple power from a pump wave (generated by an established laser) into signal and idler waves, one or both of which are in the IR. The initial source of photons for the signal or the idler can either be an existing seed laser or quantum noise. If the gain is high enough, significant conversion can occur in a single pass (e.g. parametric generation or amplification). In the case of low single-pass gain, adequate conversion may be achievable by resonantly enhancing one or more of the waves in a cavity containing the nonlinear medium (e.g. a singly or doubly resonant optical parametric oscillator – OPO). Many capable lasers exist to drive or seed nonlinear conversion to the IR. These range from compact single-frequency devices (e.g. diode-pumped solid-state lasers such as Nd:YAG) and tunable diode lasers (e.g. DFB or external-cavity diode lasers – ECDLs) to low-power lasers whose outputs are increased using fiber amplifiers or tapered-waveguide diode amplifiers [9, 10]. Capable mid-IR light sources based on birefringently phase-matched materials such as $ZnGeP_2$ [11, 12] have been successfully demonstrated.

The advent of QPM has allowed $\chi^{(2)}$ mixing to be achieved in a broader range of formats than previously possible, many of which are more amenable to chemical sensing than their birefringently phase-matched counterparts. The oft-cited benefits of QPM [13] include the ability to phase match throughout the transparency of the material, operation at higher nonlinear gain (due to freedom from walkoff and the ability to select operation at the highest nonlinear coefficient of the material), the potential for phase matching of materials that are not birefringent, and benefits afforded by patterning spectral and phase properties into the crystal. Especially important to chemical sensing are enhancements that affect system size and efficiency and the range of spectral frequencies that can be accessed. Examples of achievements exploiting the high gain of the QPM material periodically poled lithium niobate (PPLN) include the generation of practical singly resonant cw OPOs [14], the development of difference-frequency mixing systems using direct diode pumping in both bulk QPM crystals [15] and QPM waveguides [16], the development of low-threshold tunable pulsed OPOs [17–21], and the demonstration of efficient parametric amplifiers operating in the nanosecond time regime [22–24].

There have been numerous studies and applications that have taken advantage of QPM materials for gas-phase chemical sensing in the IR. These include direct absorption measurements [9, 25–27], photoacoustic measurements [28–30], Doppler-free absorption measurements [31], degenerate four-wave mixing [19], and cavity ring down spectroscopy [19, 32]. Materials used have ranged from PPLN to periodically poled KTA [33] and KTP [34].

In the remainder of this paper we present a survey of systems developed in our laboratory that employ QPM materials to advantage for performing both remote and local chemical measurements. The remote systems are laser-illuminated imaging devices that allow the real-time video visualization of gas plumes. They use either a fiber-amplifier-pumped cw PPLN OPO or a diode-seeded PPLN optical parametric amplifier (OPA) as the illuminator. The local system is a cavity ring down spectrometer that employs an OPA seeded by the filtered output of an optical parametric generator (OPG). Both the device in this system and the OPA for the imager are pumped by a compact Nd:YAG microlaser. Finally, we describe a long-wave IR difference-frequency laser that is being developed as a source for spectroscopic measurements. This new direction is particularly significant because it allows extension to the heart of the IR fingerprint region, which was not possible in the past with any practical QPM material. The performance of all of the sources and systems described is, in part, enabled by the unique properties instilled by QPM.

2 Portable gas imager employing a fiber-pumped cw OPO

Laser-illuminated gas imaging is a powerful remote-sensing technique [35] for detecting the presence and location of gas plumes. In its most basic form, gas imaging is a simple process – a scene is imaged in the IR as it is illuminated by an IR laser. The image is created using laser radiation back-scattered from solid objects in the field-of-view of the camera. If a gas capable of absorbing at the laser wavelength is present in the scene, it attenuates a portion of the back-scattered light and appears as a dark plume in the video image. As shown in Fig. 1, imagers have been constructed that are compatible with pulsed [36] or cw [35] laser illumination. In both cases, the device is designed to minimize the detection of passive thermal radiation while maximizing the collection of active (i.e. laser back-scattered) radiation. In a pulsed system, this is accomplished by illuminating all or part of the scene

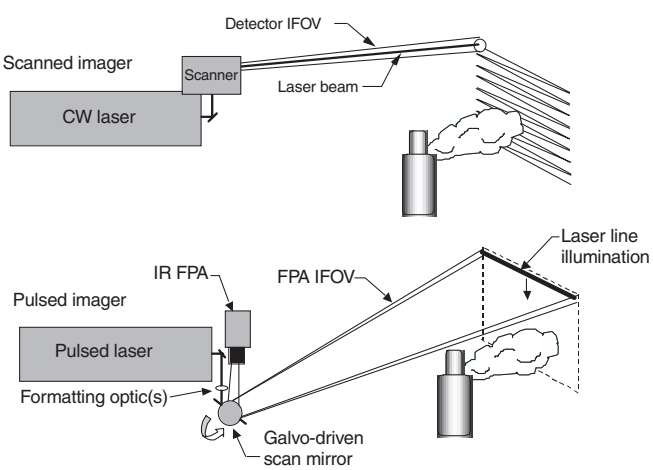

FIGURE 1 Schematic diagram of pulsed and cw laser-illuminated gas-imaging systems. The *upper system* employs a cw laser in conjunction with a raster-scanning IR camera. The system synchronously scans the laser beam and the IFOV of a single-element detector across the target in a raster pattern. The *lower system* is a pulsed line scanner. The intersection zone of the IFOV of a linear IR detector array and a fan-shaped laser illumination is swept down the target by a galvanometrically driven mirror. The laser pulses at each line on the target

with a short pulse of laser radiation and imaging that area with a gated IR focal-plane array (FPA) detector. If only part of the scene is imaged per laser shot, the laser illumination and instantaneous field-of-view (IFOV) or the array are scanned across the target to accumulate an image of the full scene with multiple laser pulses. In a cw system, the active/passive ratio is optimized by illuminating a spot in the scene with a cw laser as that spot is observed by the tightly collimated IFOV of a single-element IR detector. The intersection zone of the laser and the detector IFOV are swept across the target in a raster pattern to create the image. In both cases cold filters are used to pass only the laser wavelength to the detector.

The greatest demand for gas imaging to date exists in the natural gas and petroleum refining industries. The target species to be detected in the former is methane, the primary component of natural gas, and in the latter is a blend of organic hydrocarbons. For either effluent, the strongest IR absorptions are those attributable to the CH-stretch vibrations with maxima near 3.3-μm wavelength. The nature of the absorption spectra of these molecules varies with the size of the molecule. Methane exhibits a typical 'small-molecule' spectrum with resolved rotational lines having a pressure-broadened line width of ~ 0.1–$0.2\,\mathrm{cm}^{-1}$. Refinery hydrocarbons such as butane exhibit a 'large-molecule' spectrum in which individual rotational lines cannot be resolved and the rovibrational band has a broad (20–$40\,\mathrm{cm}^{-1}$) smooth structure. Clearly, spectral control of the laser wavelength and line width is more critical for the former application than the latter.

The first gas imagers [35, 37, 38] operated in the 9–11-μm range using CO_2 lasers and, thus, could not be applied to the refinery or natural gas problems. The lack of suitably powerful commercial lasers emitting near 3.3 μm motivated the development of laser sources for gas imaging at that wavelength. Initially, a full-field-illuminated pulsed system [36] based on the birefringently phase-matched DFG/OPA design of Milton et al. [39] was implemented. That system served as a proof-of-concept platform for pulsed imaging, but was not suitable for portable applications. Strategies considered for a more portable system included one employing a newly demonstrated PPLN-based cw singly resonant OPO [14] as an illuminator. That approach was ultimately pursued because of the lower cost of scanned single-detector-element cameras relative to the IR focal-plane arrays available at that time.

The scanned PPLN-based imager was initially implemented as a vehicle-mounted system [40] and then transformed to a battery-powered device that could be transported by a single operator. The singly resonant oscillator (SRO) used in each case is based on the bowtie-ring design of Bosenberg et al. [14], containing a 50-mm-long PPLN crystal operated at a temperature of 180 °C. In this case, the crystal is poled in a fan [41] configuration, with periods ranging from 29.3 to 30.1 μm. For the vehicle-mounted system, the OPO is pumped by a 12-W diode-pumped cw Nd:YAG laser focused to a 70-μm ($1/e^2$) beam radius in the center of the crystal. Under these conditions the OPO exhibits a threshold of 4.5 W incident on the cavity and typically produces a pump depletion of 70%. This yields at least 1.5 W of idler output over the entire tuning range of the PPLN crystal. The cavity mirrors were coated to resonate the signal wave and efficiently transmit the pump and idler radiation. Thus, the spectral profile of the idler beam resembles that of the pump beam, with a bandwidth of 10–15 GHz. This is narrow enough for refinery hydrocarbon imaging, but not well suited for measuring methane, particularly because the idler profile is composed of several separated peaks. A 100-μm-thick uncoated YAG etalon was placed in the cavity to passively stabilize the frequency of the signal wave by minimizing the frequency of mode hops. Adjustment of the position of the fan-poled PPLN crystal allows idler tuning between 3.18 and 3.53 μm (2830–$3140\,\mathrm{cm}^{-1}$), spanning most of the organic CH-stretching region.

The OPO was coupled to a raster-scanned camera and field-tested during a week-long trial at a Houston, TX petroleum refinery. At that time, the system was mounted vertically in a van, as shown in Fig. 2. The scanning camera uses galvanometrically driven mirrors to sweep the laser and the (overlapped) IFOV of a 50-μm single-element HgCdTe detector across the target at a horizontal line rate of 7866 Hz and a vertical field rate of 60 Hz. Two fields (every other line of the image) are interlaced to produce a displayed image frame. The total FOV of the system is $18 \times 14°$. The detector signal is used to assemble and display video frames of the scene at a rate of 30 frames per second. The detector IFOV is adjusted to a divergence of ~ 3 mrad and the laser divergence is set to remain within this volume. During the test, the imager was shown to be capable of displaying discernable leaks at point concentrations ranging between 2.5 and 5 percent (by volume), as verified by point measurements using a flame ionization detector.

The impracticality of operating a vehicle-mounted device within a working refinery motivated the transition to an operator-portable instrument. In addition to reduction of system size and weight, this required conversion from water to air cooling of the pump laser and a decrease of the system electrical power consumption to the point that battery-powered operation is feasible. The laser design adopted employs a cw master-oscillator power-amplifier configuration as the pump

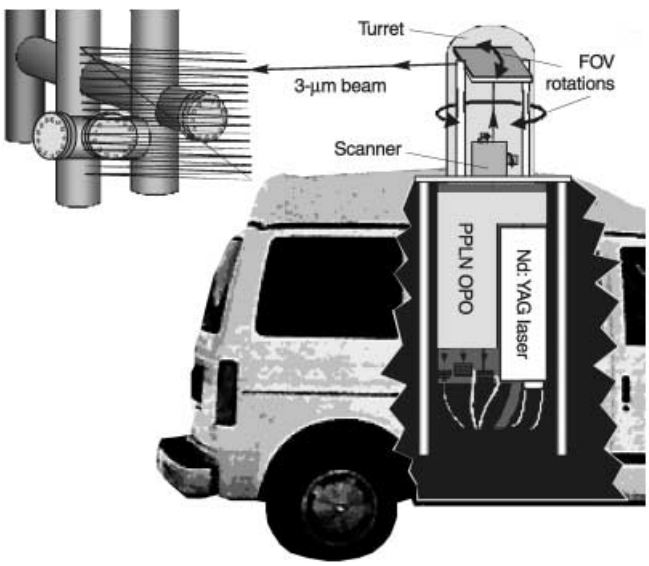

FIGURE 2 Diagram of the van-mounted, raster-scanned gas-imaging system using the Nd:YAG-pumped PPLN OPO illuminator

for the OPO. The layout of the illuminator for the portable imager is shown in Fig. 3. It consists of a miniature, single-frequency diode-pumped Nd:YAG seed laser whose output is directed into the core of a double-clad Yb-doped fiber amplifier. The amplifier is side-pumped with two 4-W single-stripe diode lasers (emitting at 975 nm), whose outputs are injected into the inner cladding of the fiber by V-groove coupling [42]. When operated at a current of 5.5 A, the amplifier is capable of generating 4.2 W of single-frequency output power at 1064 nm. The output was observed to be free of stimulated Brillouin scattering (SBS) when viewed with an optical spectrum analyzer. Although a polarization-maintaining fiber was not used, the polarization could be adjusted using a pair of waveplates and remained constant over several days of operation.

The amplifier output is coupled via a fiber pigtail to the OPO module where it is collimated as a free-space beam. To improve reliability in the field, the OPO cavity was ruggedly mounted on a single base plate. This approach allows it to be operated while the system is moved by the operator without significant fluctuation in output power. Both a reduction in the cavity length from that of the previous system and the excellent beam quality of the fiber amplifier have allowed the OPO threshold to be reduced to ~ 2.5 W. This does, however, require careful selection of the PPLN crystal as there has been some variation in crystal gain observed. When pumped with the Yb-doped amplifier at full power, the idler power ranges from 250–300 mW. At this point, the 4.2-W output power of the amplifier is sufficiently close to the OPO threshold that power drifts of the idler output can occur. This drift could be alleviated with a more powerful version of the fiber amplifier. Due to the single-mode nature of the pump, both the signal and idler output are spectrally narrow, but mode hops of the OPO cavity do occur.

The portable imager consists of two components – a shoulder-borne optical system and a power unit that is contained in a knapsack worn on the back of the operator. Figure 4 contains a photograph of the system in operation – the inset figure depicts a gas image as it appears to the operator. Also incorporated in the system are a miniature color video camera

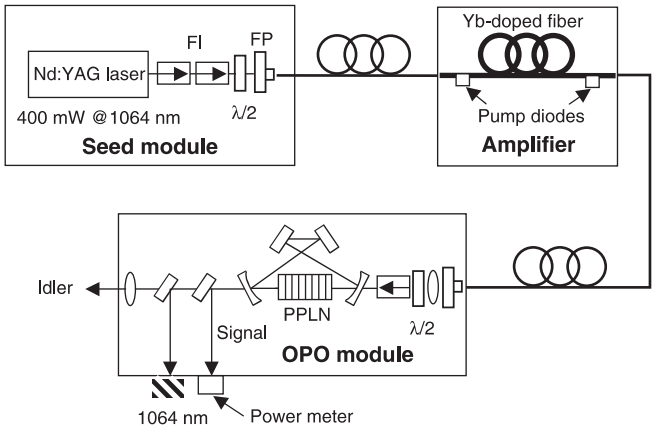

FIGURE 3 Diagram of the light source for the operator-portable gas imager. The compact cw PPLN OPO is pumped by a Nd:YAG microlaser whose output is amplified by a Yb-doped fiber amplifier. FI = Faraday isolator; $\lambda/2$ = half-wave plate; FP = FiberPort

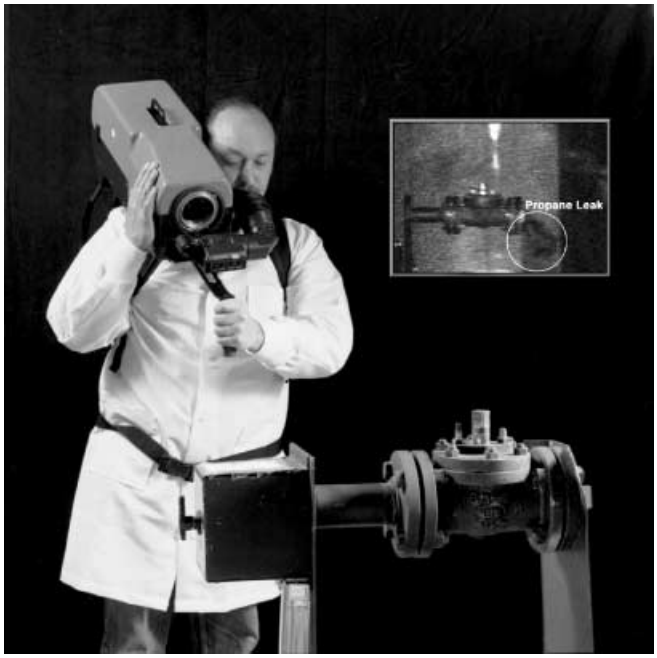

FIGURE 4 Photograph of the operator-portable gas imager in use. *Inset* shows an image of a propane gas leak produced by the system

for visible-wavelength scene display and a radio transmitter to broadcast imagery to a remote location for real-time viewing. Images can also be recorded using a compact 8-mm tape recorder worn by the operator, or by a recorder located at the remote location. Currently, the weight of the optical unit is ~ 25 pounds while that of the power unit is ~ 15 pounds.

At full OPO power, the portable system is capable of imaging at ranges up to 9 m. The collection efficiency of its receiver is increased through the use of scan mirrors that are a factor of two larger than those used in the van-mounted system, which compensates for the lower power of the compact OPO. The diode pump lasers for the fiber amplifier and elements within the seed laser require thermoelectric cooling to maintain their operating temperatures. Heat is removed from the system via forced air flow through both the optical system chassis and the power unit. The total power draw of the system ranges from 200 to 240 W, depending on the ambient air temperature.

The efficient cw operation of both systems described above is owed to the use of a QPM material in conjunction with effective pump lasers. The high gain of PPLN enables operation of a high-depletion cw OPO that would not have been possible previously in a singly resonant format using birefringently phase-matched materials. Similarly, it produces an output power at 3.3 μm that is not achievable with any commercially available diode lasers. Finally, the ability to pattern spectral information into the crystal eases the complexity of tuning the idler wavelength, which is accomplished by a simple translation of the crystal.

3 Gas imager employing a diode-seeded, microlaser-pumped OPA

The high nonlinear drive of PPLN also allows efficient single-pass generation of pulsed IR light. A single-pass OPG or OPA is simpler to implement than an OPO

because it does not require an optical cavity. Moreover, tuning is facilitated if the process is seeded by a laser that is already engineered to tune easily. While earlier OPGs or OPAs required the high pump intensities of picosecond light sources or tens of mJ of pump energy in the nanosecond regime [43], PPLN-based single-pass devices have been shown to achieve significant conversion when pumped with extremely compact nanosecond sources, such as Nd:YAG microchip lasers [22, 24]. Nanosecond pulse lengths are preferable to shorter pulses for gas-phase chemical measurements in the IR because their transform-limited line widths allow resolution of individual rotational lines.

In order to meet the Japanese natural gas industry's goal to accelerate surveillance for indoor natural gas leaks, a handheld methane imager using a seeded PPLN OPA is being constructed. This device is intended for short (5 m) standoff detection at a sensitivity of 10 ppm-m path-integrated methane concentration. The method of measurement of this imager differs from that of the cw system because it is capable of operating in a single- or dual-wavelength mode. The latter, termed differential imaging [44], is carried out by illuminating each pixel in an image with radiation at two wavelengths – one resonant with the gas to be detected (termed the 'on wavelength') and one not resonant (termed the 'off wavelength'). Prior to display, the differential image is created by ratioing the on-wavelength signal to the off-wavelength signal and displaying the logarithm of the result. This removes imagery of the background scene and leaves the image of the gas plume. Because only the plume image remains, it is possible to view it more clearly than in the relatively cluttered single-wavelength image. Differential imaging is analogous to a topographic-backscatter differential absorption lidar (DIAL) measurement made in two dimensions.

Several illumination strategies for the handheld imager were considered according to the ease of pumping and tuning of the laser source, and the minimization of systematic errors in the imaging process. The configuration selected is a pulsed line scanner, illustrated in Fig. 1. It emits a pulse of IR radiation that is shaped to illuminate a line on the target, and images the backscatter from that line onto a 256-element linear focal-plane array detector. The intersection zone of the line illumination and the line detection is swept down the scene using a galvanometrically driven scan mirror.

The light source selected for this system is a PPLN OPA that is pumped by the output of a Nd:YAG microlaser and seeded by a DFB diode laser operating at 1577.3 nm. This system is illustrated in Fig. 5. The microlaser is a 3-mm-diameter monolithic rod consisting of a four separate sections – a 7-mm-long Nd-doped gain region, a 1-mm-long undoped end cap fused to the pumped end of the gain region, a 1.7-mm-long Cr-doped passive Q-switch, and an 8-mm-long undoped spacer region (between the Q-switch and the output face). The Q-switch is centrally located to ensure single-longitudinal-mode operation. The end cap serves as a heat-dissipation zone to prevent thermal fracture of the rod end due to absorption of the pump radiation. The ends of the microlaser are coated to reflect the 1064-nm resonated radiation and to transmit the 810-nm pump radiation.

The microlaser is pumped by the output of a 12-W fiber-coupled diode bar emitting at 810 nm. The rod is end-pumped by focusing the output of the multi-mode fiber into the end-capped face. The pump provides 270-μs-long pulses at a rate of 1 kHz, with each pulse resulting in the emission of two microlaser output pulses of $\sim$ 2.6-ns duration at 1064-nm wavelength, spaced 100-μs apart. The energy of these pulses has been measured to be 75 μJ (±0.3%) for the first and 85 μJ (±1.5%) for the second. Each pulse originates from a single longitudinal mode of the cavity and exhibits linear polarization along the same axis. A difference in frequency of $\sim 0.29\,\mathrm{cm}^{-1}$ has been observed between these pulses, which may be attributed to heating of the rod during the first pulse.

The OPA consists of a 50-mm-long piece of 1-mm-thick PPLN, poled with a period of 29.7 μm. The microlaser output is injected into the crystal collinearly with the output of the DFB diode laser. The pump beam forms a waist ($1/e^2$ radius) of 30 μm in the crystal. The OPA exhibits the performance shown in Fig. 6, with a threshold of $\sim$ 20 μJ and an efficiency of $\sim$ 9% in idler output when pumped at the $\sim$ 80-μJ output of the microlaser. This yields 5.5 μJ (±0.3%) for the first idler pulse and 5.9 μJ (±0.5%) for the second. Note that when the OPA is pumped at energies achievable with the microlaser, the onset of backconversion can be achieved in a single pass. Thus, there is no need for resonant feedback (i.e. an OPO). The line width of the OPA idler output has been measured to be $\leq 0.05\,\mathrm{cm}^{-1}$, which is significantly

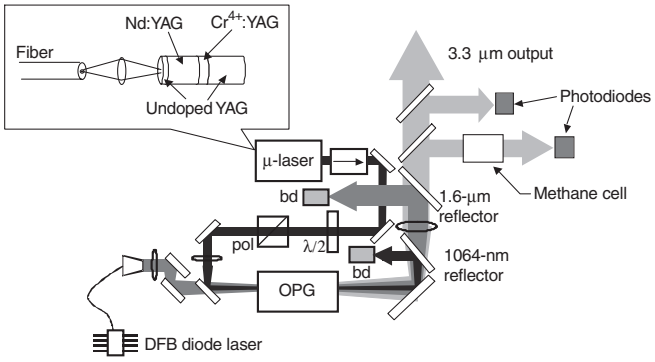

FIGURE 5 Diagram of the microlaser-pumped, diode-seeded OPA used in the pulsed line-scanned gas imager. bd = beam dump; λ/2 = half-wave plate; pol = polarizer

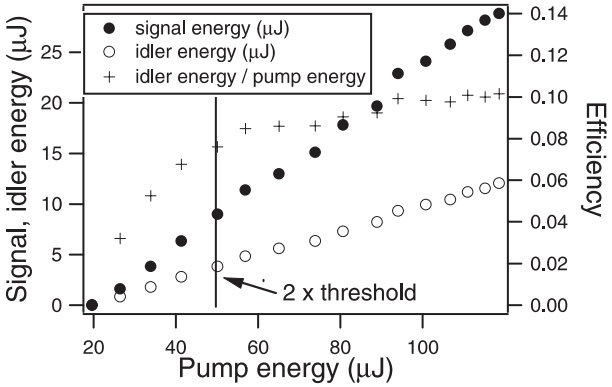

FIGURE 6 Graph of the signal and idler energies produced by the OPA and the efficiency of the OPA as a function of pump energy

narrower than the width of the methane absorption line selected for measurement (the R-branch rovibrational line at 3270.4 nm).

The process of image formation takes advantage of the double-pulse operation of the OPA. In performing differential imaging, it is essential that the data collected at the on- and off-wavelengths are well registered both spatially and temporally. If this is not the case, changes in contrast resulting from illumination of slightly different regions of the target will lead to errors in the differential signal. Proper registration is ensured by using a galvanometer that is capable of scanning in discrete steps. The galvanometer is stepped so that the aiming point of the OPA and the linear FPA remains stationary at the target during the 100-μs time interval in which a pair of pulses is emitted. The DFB laser current is adjusted so that the spectral frequency of the first member of the pulse pair corresponds to an on line and the second to an off line. The short time between pair pulses also makes it unlikely that camera motion or motion of the target will lead to deregistration of the on- and off-wavelength pulses. Following the last pulse of a pair, 450 μs is allowed for the scan mirror to direct the aim point to the next line on the image. After the last line is collected, the galvanometer mirror rapidly retraces to the top of the target area for initiation of the next frame. When operated in single-wavelength mode, the double pulsing of the OPA must be compensated for by scanning the galvanometer in an irregular fashion, in which line steps are made more rapidly between members of a pair than they are between pairs. This ensures evenly spaced illumination lines.

To produce high-contrast images of methane plumes, it is necessary to precisely control the idler wavelength to a value near the peak of the methane absorption. This is accomplished using an active frequency-stabilization procedure that regulates the DFB laser wavelength. In order to compensate for pump and seed laser drifts, it is necessary to generate an error signal directly from the idler beam. As shown in Fig. 5, a portion of the idler beam is passed through a small cell containing methane and sensed by a room-temperature InAs detector. When locked, the OPA has been shown to maintain the idler frequency at a value corresponding to $\geq 90\%$ of that at the line peak (i.e. within 2.2 GHz of line center). The position of the idler can also be set to the off wavelength on the second pulse of each pair when the differential mode is used. In all cases, frequency control is greatly facilitated by the use of a single-pass QPM frequency converter where the seed laser can be freely adjusted without consideration of cavity modes. The laser operation and locking will be discussed in more detail in a forthcoming publication [45].

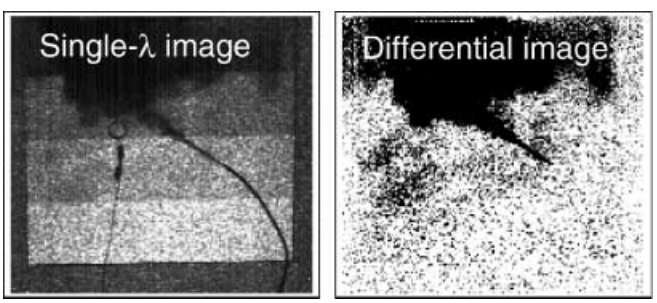

FIGURE 7 Single-wavelength and differential images created by the pulsed line-scanned gas imager

At the present time, the imager is operating in a breadboard format at a frame rate of 3 Hz for both single-wavelength and differential imaging operation. Figure 7 contains imagery collected by that system in each format at a standoff range of ~ 2 m. The OPA was used to illuminate the FOV of a 256×1 region of a 320×256 InSb FPA (only one line of the two-dimensional array is used) that was gated to integrate for $\sim 10\,\mu$s at a time synchronous with the pulsing of the OPA. This window is sufficiently wide to compensate for temporal fluctuations of the pump laser resulting from the use of a passive Q-switch and due to the double-pulse nature of the operation. The OPA is pulsed at a pair frequency of 1000 Hz. This yields a vertical resolution of 188 lines while the horizontal resolution is fixed to 256 pixels by the dimensions of the FPA region used.

In the near future, a faster galvanometer will be incorporated into the system to allow the frame rate to be increased to 20 Hz for single-wavelength operation and 10 Hz for differential imaging. In addition, the system will be packaged into two modules – a handheld imaging package and a backpack power unit.

4 Cavity ring down spectrometer using a filtered two-stage OPA

The tuning range of the OPA described above can be extended to allow its use as a spectroscopic light source by employing a more broadly tunable seed laser and increasing the range of available PPLN periodicity. Two candidate seed sources are a more widely tunable diode laser (e.g. an ECDL) or a narrow seed generated from the filtered output of a high-brightness, broadband light source. The latter approach was selected for the sensor described here, with a PPLN OPG serving as the broadband emitter [23]. The OPG consists of a PPLN crystal that is pumped at sufficient intensity to generate useable levels of parametric fluorescence from quantum noise. The spectral width of the parametric fluorescence is set by the phase-matching bandwidth of the PPLN crystal used. A seed-laser pulse is sculpted from this emission by spectrally filtering the signal beam from the OPG through a piezoelectrically tunable etalon. Fine tuning of this seed pulse is accomplished by tuning the etalon within the bandwidth of a given PPLN period; broader tuning is achieved by translating the PPLN crystal to access new periods or by temperature tuning the crystal. At a given periodicity the bandwidth of the signal beam is determined by the narrow-band filter and the idler bandwidth is the convolution of the signal and the pump. A single-frequency pump laser combined with the narrow-band seeding results in a narrow bandwidth for both the signal and idler, making both outputs suitable for spectroscopy. This cascaded OPG-OPA has been used as a light source for a broadly tunable and compact pulsed cavity ring down spectrometer.

Cavity-ring down spectroscopy (CRDS) is a high-sensitivity method of measuring loss in an optical cavity, and has been described in numerous publications (see, for example, [46]). One or more modes of a high-finesse cavity are loaded with radiation from a laser and, upon termination of the input ra-

diation, the subsequent rate of loss of light (ring down) from the cell is monitored. This is insensitive to shot-to-shot energy fluctuations and makes possible high signal-to-noise measurements. When applied to gas-phase spectroscopic measurements, the high-finesse ring down cavity is filled with a gas to be analyzed and the loss is measured as a function of laser wavelength. The difference between this loss spectrum and that of the empty cell yields the loss spectrum of the gas sample, which can be related to sample absorbance. Pulsed CRDS is well matched to the performance of the OPG-OPA because it allows high-sensitivity measurements to be made with low-energy ($\sim \mu$J) pulses.

A diagram of the CRDS spectrometer is shown in Fig. 8. The OPG-OPA has been pumped with the output of either one of two laser sources – an injection-seeded, diode-pumped Nd:YAG laser (Continuum HPO-1000) emitting 15-ns-long pulses at a repetition rate of 1 kHz, or a microlaser similar to that described in Sect. 3. Here, however, the microlaser is pumped with 60-W pulses of diode pump light having a duration of 200 μs. These pulses are delivered to the microlaser at a rate of 120 Hz, which results in the emission of single 1064-nm output pulses with an energy of $\sim 650\,\mu$J. Again, these pulses are linearly polarized, have a duration of 2.6 ns, and are the result of lasing on a single longitudinal cavity mode.

As shown in Fig. 8, the pump laser output is split to pump both the first and second stages of the IR converter. Each stage consists of a 50-mm-long PPLN crystal. The system has been implemented with each crystal poled in either a step- or fan-shaped pattern, and crystal bandwidth tuning is accomplished in each case through a combination of crystal translation and/or temperature tuning. When pumped with the short-pulse microlaser, the first stage receives 100 μJ of energy at 1064 nm focused to a waist (intensity $1/e^2$ radius) of 190 μm. This results in an OPG threshold of $\sim 70\,\mu$J. At 100-μJ pump energy, the signal pulse has an energy of $\sim 8\,\mu$J and a bandwidth of $\sim 15\ \mathrm{cm}^{-1}$.

Spectral narrowing of the signal output of the first stage is accomplished by passing it through a piezoelectrically tunable, air-spaced Fabry–Perot etalon having a maximum finesse of 450 at a wavelength of 1.55 μm. The free spectral range of the etalon was adjusted to span a breadth slightly wider than the gain bandwidth of the PPLN crystal. Again, for the case of the microlaser, the filtered signal is then focused to a beam radius of 460 μm in the OPA crystal where it overlaps with the pump beam, which is focused to a radius of 410 μm. Under these conditions, 10 μJ of spectrally narrow idler output is produced (and 30-μJ signal). The line width was determined to be $0.05\ \mathrm{cm}^{-1}$ through measurement of a narrow spectral feature.

To perform CRDS, the idler output beam is matched to the lowest-order spatial mode of a linear 46.5-cm base-path length ring down cell. The cell consists of a pair of plano-concave mirrors having a 6-m radius of curvature and coated to be 99.98% reflective at 3.3 μm. The cell was housed in a stainless-steel jacket (with CaF_2 windows that transmitted the input and output radiation) that could be evacuated and filled with a gas to be measured. Radiation transmitted from the end of the ring-down cell was collected and focused onto a 1-mm-diameter liquid-nitrogen-cooled InSb detector. The detector signal was amplified by a 150-MHz video preamplifier and digitized by a fast (80 M samples/s) 12-bit analog-to-digital conversion card that was used for collecting ring-down traces at repetition rates up to 1 kHz.

The seeded OPA provides many advantages for CRDS over competing light sources. The relatively low pump energy required makes it possible to drive the system with high-repetition-rate (i.e. low energy) diode-pumped solid-state lasers. This is an efficient way to collect pulsed CRDS data because it increases the fraction of time that the cell is actually making a measurement relative to the duty cycle of lower-repetition-rate systems based on flashlamp-pumped Nd:YAG lasers. The noise floor that is achieved using the described setup is $1.3 \times 10^{-8}\ \mathrm{cm}^{-1}$ ($2.9 \times 10^{-8}\ \mathrm{cm}^{-1}\ \mathrm{Hz}^{-1/2}$) loss per pass in the cell. This was measured using the 1-kHz-repetition-rate laser with an 800-point running average (0.8 s). Figure 9 illustrates the spectral scanning rate that can be achieved with that configuration. With no data averaging at a 1-kHz collection rate, one PPLN gain segment ($\sim 15\ \mathrm{cm}^{-1}$)

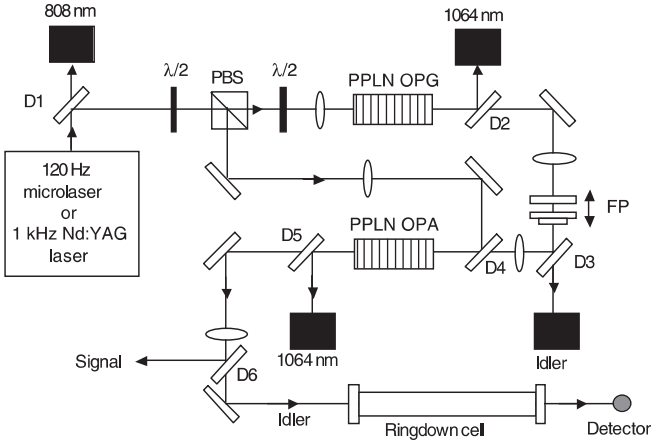

FIGURE 8 Diagram of the OPG-OPA light source for the CRDS instrument. D1 – 6 = dichroic filters; PBS = polarizing beam splitter; FP = Fabry–Perot etalon; λ/2 = half-wave plate

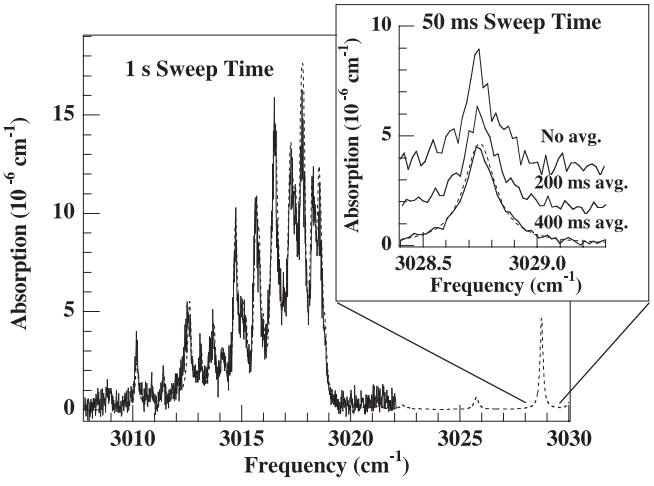

FIGURE 9 Spectra indicating the speed of data collection of the CRDS instrument using the 1-kHz pump source. The data shown were taken with no averaging. In each case the gas measured is methane at a concentration of 500 ppb in nitrogen (at 760 torr). The data collected are overlaid with a spectrum calculated using HITRAN (*dashed line*)

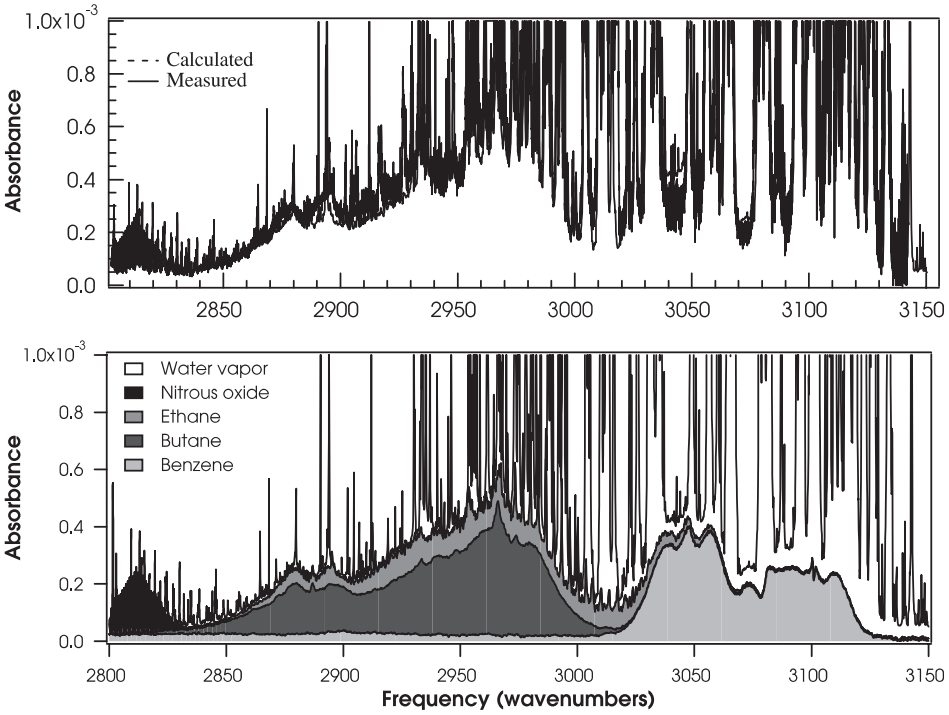

FIGURE 10 Long CRDS scan of a gas mixture consisting of benzene, butane, ethane, nitrous oxide, and water vapor at the concentrations indicated in the text. The scan was assembled from 27 individual scan segments. The *bottom plot* shows the calculated total spectrum and the contribution from the individual chemical constituents. The *top plot* shows the calculated spectrum overlaid with the measured spectrum

can be scanned in about 1 s. As shown in Fig. 9, this allows measurement of the Q-branch of methane in one second with a detection limit of $\sim$ 20 ppb for the peak of the feature. A scan of a single rotational line can be achieved in a sweep time of 50 ms with no data averaging.

The combination of etalon and PPLN period tuning allows spectral scanning over ranges much broader than are achievable using other compact laser sources (e.g. diode lasers). This is illustrated in Fig. 10 where a segmented scan over a 350-cm^{-1} width is shown. The spectrum consists of a mosaic of 27 scan segments. The data shown are the result of the subtraction of a full cell scan from an empty cell scan. The species present in the mixture are nitrous oxide (50 ppm), butane (324 ppb), benzene (1.69 ppm), ethane (540 ppb), and water vapor (40% RH at 23 °C).

Some additional aspects of the performance of the PPLN-based CRDS instrument can be observed in Fig. 10. The breadth of the scan allows capture of the 'large-molecule' unresolvable bands of butane and benzene. Provided sufficient PPLN periods were available, the source tuning could be extended over the full range of 1.3–4.3 μm dictated by the PPLN transparency. It is, however, a laborious process to collect and register tens of scan segments to generate a broad scan. The need to mosaic scans is currently required for two reasons – the first being the need to adjust PPLN periodicity and the second to change etalon order. The first can be alleviated by mechanically stepping a fan-poled PPLN crystal in synchrony with the tuning of the spectral filter. The latter requires a spectral filter with a larger continuous tuning range. As a candidate for the latter, we have explored the use of a high-finesse microcavity etalon developed for the telecommunications industry (Micron Optics, Atlanta, GA). That device was designed with a very high finesse ($\sim$ 2000) and large free spectral range (200 cm^{-1}). It was possible to demonstrate continuous tuning with that device over $\sim$ 200 cm^{-1}; however, the etalon was susceptible to damage by the high seed powers incident on the microcavity. If this problem can be resolved, it will allow seamless tuning over ranges similar to that in Fig. 10 and will greatly accelerate the scanning process

5 Development of long-wave IR sources using QPM GaAs

Arguably, the most desirable wavelengths at which to make local or remote spectral measurements in the fundamental absorption range of the IR are in the so-called 'fingerprint' [2] region between 8 and 15 μm. There, small changes in the structure and constitution of a molecule yield the largest changes in the absorption spectrum, due to the wide diversity of functional groups that are active in that window. In contrast, the mid-wave IR (3–5 μm) contains absorptions due primarily to stretching motions of hydrogen-containing functionalities (e.g. CH, OH, NH). Spectral features associated with those structures are often indistinct and provide little information about the skeletal makeup of the molecule. There are additional advantages to operating in the long-wave IR, including the fact that the modes that absorb there generally have higher cross section and that the long-wave atmospheric window is freer from water vapor absorption than the mid-wave window.

All ferroelectrically poled QPM materials demonstrated to date are unusable in the fingerprint region because of material absorption. This has motivated the consideration of other nonlinear materials and other means of creating QPM structures. One material investigated is GaAs, which transmits in the range of 0.9–17 μm and exhibits a higher nonlinear coefficient (values reported between 83 [47] and 150 [48] pm/V). GaAs is a good candidate for phase matching via QPM because it cannot be birefringently phase-matched. Also, because it cannot be ferroelectrically poled, other means of creating the QPM structure are required.

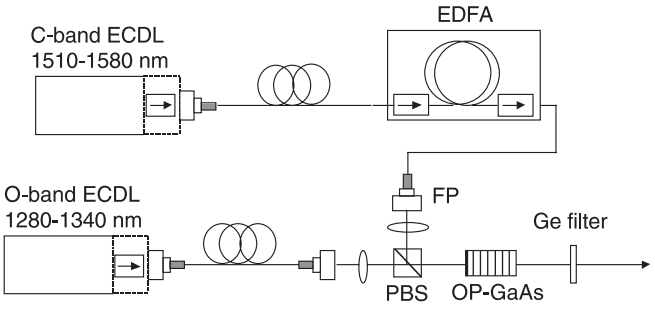

FIGURE 11 Diagram of the long-wave difference-frequency spectrometer employing OP-GaAs. EDFA = erbium-doped fiber amplifier; PBS = polarizing beam splitter; FP = FiberPort

The most versatile method to date for creating bulk QPM GaAs was developed by Eyres et al. [49]. It is based on the fabrication of a spatially patterned template that serves as a seed crystal for the subsequent upward growth of a patterned bulk crystal. The fabrication of the seed crystal takes place through a combination of molecular-beam epitaxial growth, photolithography, and etching steps. The thick-film growth occurs using a hydride vapor transport process. The product is referred to as orientation-patterned GaAs (OP-GaAs). Previously developed alternate methods for phase matching GaAs include the diffusion bonding of oriented stacks of thin GaAs plates [50, 51], exploitation of the phase shift occurring upon total internal reflection in GaAs plates [52, 53], and early patterning attempts leading to QPM waveguide fabrication [54].

In collaboration with Stanford University, we have obtained samples of OP-GaAs and implemented them in a tunable long-wave IR light source [55]. That device is illustrated in Fig. 11 and consists of a cw difference-frequency mixer in which the outputs of two tunable ECDLs operating in the telecommunications bands near 1550 nm and 1310 nm are subtracted. Each ECDL is coarsely ($\sim 0.2\,\mathrm{cm}^{-1}$ resolution) tunable over ~ 70 nm via stepper-motor tilting of the Littman cavity mirror, and finely tunable over ~ 1–$2\,\mathrm{cm}^{-1}$ through fine adjustment of the mirror tilt using a piezoelectric element. The 1550-nm beam is injected into a polarization-maintaining fiber amplifier to increase its power to 1 W. The 1310-nm laser is used without amplification at a power of 1–3-mW output. Pump tuning is possible over a range of 1.27–1.34 μm while signal tuning is limited to 1.53–1.57 μm by the gain bandwidth of the fiber amplifier. Each beam is launched in free space to a polarizing beam-splitter cube, where they are combined and directed toward the crystal. The polarizations of beams launched to the crystal are orthogonal, as required for coupling via the d_{14} nonlinear coefficient of the QPM GaAs. The signal and pump beams are focused into the crystal to obtain confocal focusing conditions at the idler wavelength. The GaAs QPM period is 26.3 μm, and the sample was 19-mm long, 5-mm wide, and 0.5-mm thick with over 80% of the interaction length free of defects.

The power of the idler beam produced was between 30 and 100 nW for input powers of 1–3 mW and 1-W input power at 1.3 and 1.55 μm respectively. These values agree with the theoretical prediction made assuming that the nonlinear coefficient of OP-GaAs is 90 pm/V and taking into consideration the fraction of defects present in the crystal. Work is now underway to add amplification of the 1.3-μm channel in order to increase the idler output power to the μW range.

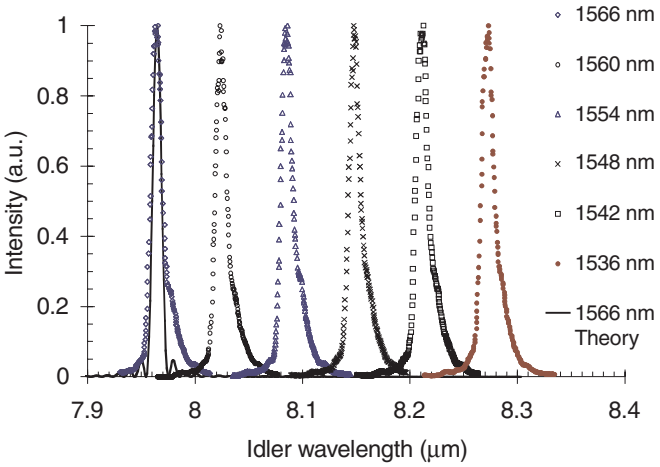

FIGURE 12 Tuning of the idler output of the OP-GaAs DFG system as a function of signal wavelength. For each curve, the signal wavelength was set at the value indicated in the *legend* and the pump wavelength was adjusted to achieve phase matching

Figure 12 shows the tuning behavior of the idler beam. Each curve was obtained with the signal set to the indicated wavelength and the pump tuned across the phase-matching profile of the crystal. The operating range of this crystal can be extended via temperature tuning as shown in Fig. 13. There the signal wavelength was set to 1.536 μm and the pump was tuned over the phase-matching profile for five temperatures ranging from 30 to 110 °C. The overall frequency range accessible for this periodicity in the long-wave IR thus ranges from 7.95 to 8.6 μm (1160 to 1260 cm^{-1}). This is about 10 times the tuning range that can be achieved for available DFB QC diode lasers.

As can be inferred from Fig. 13, the phase-matching bandwidth of OP-GaAs is quite narrow (2–3.5 cm^{-1}) at the wavelengths used. Broad continuous tuning can, however, be accomplished by concerted tuning of the pump and signal laser beams. Figure 14 contains a plot of the tuning that could be achieved with the pump sources used if crystals of the appropriate period were available. Using seven

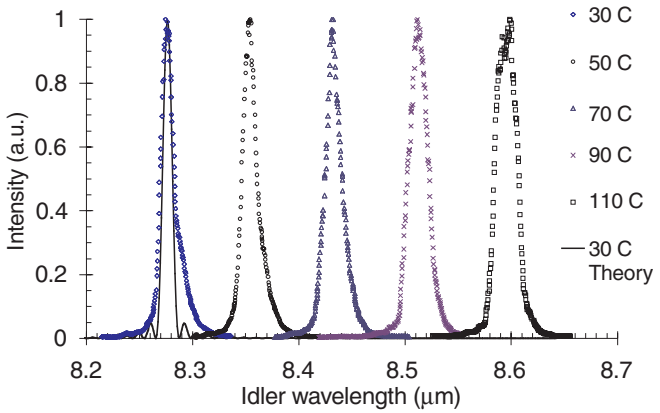

FIGURE 13 Tuning of the idler output of the OP-GaAs DFG system as a function of temperature. For each curve, the signal crystal temperature was set at the value indicated in the *legend* and the pump wavelength was adjusted to achieve phase matching. The signal wavelength was 1.536 μm in all cases

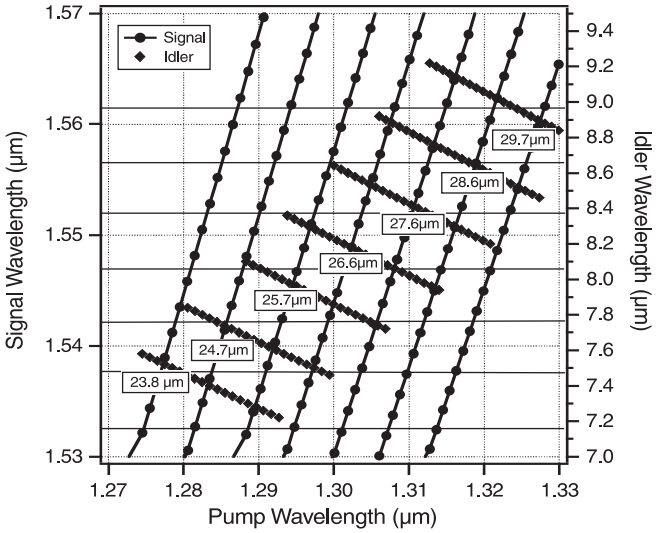

FIGURE 14 Diagram showing the full tuning possible with the pump and signal sources for the indicated OP-GaAs periodicities at a temperature of 25 °C. The *near-vertical lines* show the signal phase matching as a function of pump wavelength. The *near-horizontal lines* show the idler tuning

Band	Wavelength range (μm)	O-band wavelength (μm)
O	1.260–1.360	–
S	1.460–1.530	7.14–19.9
C	1.525–1.565	6.46–12.7
L	1.565–1.625	5.61–10.4
U	1.625–1.675	5.09–8.34

TABLE 1 Long-wave IR tuning allowed by differencing telecom frequency windows

crystal periodicities ranging from 23.8 to 29.7 μm, it would be possible to cover the idler range from 7.2 to 9.2 μm (1090–1390 cm^{-1}) with considerable spectral overlap among adjacent periods.

There is great benefit in exploiting available pump laser technology from the telecommunications industry due to the investment made in engineering those products and their associated hardware. It is interesting to consider the wavelengths accessible when starting with lasers from the other telecom wavelengths. Table 1 contains a listing of the primary telecom channels and the frequencies that can be generated by differencing O-band lasers with the other bands. The system described above employs O- and C-band lasers (although they are not tunable over the full range of those bands). From the table, it appears that the O–S choice appears to be optimal for covering the full molecular fingerprint region.

6 Summary and conclusions

The execution of practical optical measurements mandates laser sources that are simple, rugged, and efficient. In this paper we have described several instances in which the use of QPM devices allows spectroscopically useful IR radiation to be produced in a manner that is consistent with these goals, and have shown examples of measurements and instrumentation made with these light sources. Aspects of QPM performance that are relevant include the ability to produce sufficient conversion on a single pass (thus avoiding the complexity of a resonator), the ability to seed the single-pass process in a frequency-agile manner, the efficient conversion of cw light, and the simplicity afforded by patterned spectral properties. These benefits are complemented by the availability of effective pump lasers such as high-power, high-mode-quality fiber amplifiers or Nd:YAG microlasers. Clearly, the incorporation of highly engineered products from the telecom industry further advances the goals of sensing at very little cost.

Of particular interest for the future is the extension of the spectral coverage to include the full mid-to-long-wave IR through the use of patterned semiconductor materials such as GaAs. The broad tunability, room-temperature operation, spectral formatting, and wide variety of temporal/energy formats will allow these nonlinear devices to complement the advances being made in IR semiconductor technology.

ACKNOWLEDGEMENTS The work represented in this paper was funded by several sources, which include the U.S. Department of Energy Offices of Fossil Energy, Industrial Technologies, Non-proliferation, and National Security, the Office of Research and Development, and the Gas Research Institute. The authors gratefully acknowledge METI for sponsorship of the development of the handheld gas imager. The authors also acknowledge the assistance of the Japan Gas Association Staff, Dr. Kiran Kothari of the Gas Research Institute and the valuable advice provided by Dr. Takao Kobayashi, Dr. Hiroaki Kuze, and Dr. Nobuo Sugimoto.

REFERENCES

1 M.M. Fejer, G.A. Magel, D.H. Jundt, R.L. Byer: IEEE J. Quantum Electron. **QE-28**, 2631 (1992)
2 D.A. Skoog, F.J. Holler, T.A. Nieman: *Principles of Instrumental Analysis* (Harcourt Brace, Orlando, FL 1998) pp. 404–428
3 P. Werle, F. Slemr, K. Maurer, R. Kormann, R. Mucke, B. Janker: Opt. Lasers Eng. **37**, 101 (2002)
4 M. Tacke: Infrared Phys. Technol. **36**, 447 (1995)
5 A. Fried, B. Henry, S. Sewell, J.R. Drummond: Appl. Phys. B **67**, 317 (1998)
6 F. Capasso, A. Tredicucci, C. Gmachl, D.L. Sivco, A.L. Hutchinson, A.Y. Cho, G. Scamarcio: IEEE J. Sel. Top. Quantum Electron. **5**, 792 (1999)
7 C. Gmachl, F. Capasso, R. Kohler, A. Tredicucci, A.L. Hutchinson, D.L. Sivco, J.N. Baillargeon, A.Y. Cho: IEEE Circuits Dev. **16**, 10 (2000)
8 M. Beck, D. Hofstetter, T. Aellen, J. Faist, U. Oesterle, M. Ilegems, E. Gini, H. Melchior: Science **295**, 301 (2002)
9 F.K. Tittel, D.G. Lancaster, D. Richter: Laser Phys. **10**, 348 (2000)
10 U. Simon, F.K. Tittel, L. Goldberg: Opt. Lett. **18**, 1931 (1993)
11 K.L. Vodopyanov: Laser Focus World, May, 225 (2001)
12 F. Ganikhanov, T. Caughey, K.L. Vodopyanov: J. Opt. Soc. Am. B **18**, 818 (2001)
13 L.E. Myers, W.R. Bosenberg: IEEE J. Quantum Electron. **QE-33**, 1663 (1997)
14 W.R. Bosenberg, A. Drobshoff, J.I. Alexander, L.E. Myers, R.L. Byer: Opt. Lett. **21**, 1336 (1996)
15 D. Richter, D.G. Lancaster, R.F. Curl, W. Neu, F.K. Tittel: Appl. Phys. B **67**, 347 (1998)
16 K.P. Petrov, A.P. Roth, T.L. Patterson, T.P.S. Thoms, L. Huang, A.T. Ryan, D.J. Bamford: Appl. Phys. B **70**, 777 (2000)
17 G.W. Baxter, P. Schlup, I.T. McKinnie: Appl. Phys. B **70**, 301 (2000)
18 S.T. Yang, S.P. Velsko: Opt. Lett. **24**, 133 (1999)
19 G.W. Baxter, M.A. Payne, B.D.W. Austin, C.A. Halloway, J.G. Haub, Y. He, A.P. Mice, J. Nibler, B.J. Orr: Appl. Phys. B **71**, 651 (2000)
20 B.A. Richman, K.W. Aniolek, T.J. Kulp, S.E. Bisson: J. Opt. Soc. Am. B **17**, 1233 (2000)
21 Y. He, B.J. Orr: Appl. Opt. **40**, 4836 (2001)
22 J.J. Zayhowski: Opt. Lett. **22**, 169 (1997)
23 P.E. Powers, K.W. Aniolek, T.J. Kulp, B.A. Richman, S.E. Bisson: Opt. Lett. **23**, 1886 (1998)
24 K.W. Aniolek, R.L. Schmitt, T.J. Kulp, B.A. Richman, S.E. Bisson, P.E. Powers: Opt. Lett. **25**, 557 (2000)

25 K.P. Petrov, S. Waltman, E.J. Dlugokencky, M. Arbore, M.M. Fejer, F.K. Tittel, L.W. Hollberg: Appl. Phys. B **64**, 567 (1997)
26 M. Seiter, M.W. Sigrist: Infrared Phys. Technol. **41**, 259 (2000)
27 K.P. Petrov, A.T. Ryan, T.L. Patterson, L. Huang, S.J. Field, D.J. Bamford: Opt. Lett. **23**, 1052 (1998)
28 S.E. Bisson, K.M. Armstrong, T.J. Kulp, M. Hartings: Appl. Opt. **40**, 6049 (2001)
29 C. Fischer, M.W. Sigrist, Q. Yu, M. Seiter: Opt. Lett. **26**, 1609 (2001)
30 F. Kuhnemann, K. Schneider, A. Hecker, A.A.E. Martis, W. Urban, W. Schiller, J. Mlynek: Appl. Phys. B **66**, 741 (1998)
31 E.V. Kovalchuk, D. Dekorsy, A.I. Lvovsky, C. Braxmaier, J. Mlynek, A. Peters, S. Schiller: Opt. Lett. **26**, 1430 (2001)
32 K.W. Aniolek, P.E. Powers, T.J. Kulp, B.A. Richman, S.E. Bisson: Chem. Phys. Lett. **302**, 555 (1999)
33 K. Fradkin Kashi, A. Arie, P. Urenski, G. Rosenman: Opt. Lett. **25**, 743 (2000)
34 G.M. Gibson, M. Ebrahimzadeh, M.J. Padgett, M.H. Dunn: Opt. Lett. **24**, 397 (1999)
35 T.G. McRae, T.J. Kulp: Appl. Opt. **32**, 4037 (1993)
36 T.J. Kulp, P. Powers, R. Kennedy, U.B. Goers: Appl. Opt. **37**, 3912 (1998)
37 T.J. Kulp, R. Kennedy, M. Delong, D. Garvis, J. Stahovec: Proc. SPIE, Appl. Laser Radar Technol., Orlando, FL (Society of Photo-Optical Instrumental Engineers, Bellingham, WA 1993) pp. 204–213
38 T.J. Kulp, P.E. Powers, R. Kennedy: Proc. SPIE, Infrared Technol. Appl. XXIII, Orlando, FL, Vol. 3061 (Society of Photo-Optical Instrumental Engineers, Bellingham, WA 1997) pp. 269–278
39 M.J.T. Milton, T.J. McIlveen, D.C. Hanna, P.T. Woods: Opt. Commun. **93**, 186 (1992)
40 U.B. Goers, T.J. Kulp, P.E. Powers, T.G. McRae: SPIE Proc. **3758**, 172 (1999)
41 P.E. Powers, T.J. Kulp, S.E. Bisson: Opt. Lett. **23**, 159 (1998)
42 J.P. Koplow, L. Goldberg, D.A.V. Kliner: IEEE Photon. Technol. Lett. **10**, 793 (1998)
43 S. Wu, V.A. Kapinus, G.A. Blake: Opt. Commun. **159**, 74 (1999)
44 P.E. Powers, T.J. Kulp, R. Kennedy: Appl. Opt. **39**, 1440 (2000)
45 T.A. Reichardt, R.P. Bambha, T.J. Kulp: to be submitted to Opt. Lett. (2002)
46 K.W. Busch, M.A. Busch: *Cavity-Ringdown Spectroscopy: An Ultratrace Absorption Measurement Technique* (ACS Symp. Ser. 720) (American Chemical Society, Washington DC 1999)
47 I. Shoji, T. Kondo, A. Kitamoto, M. Shirane, R. Ito: J. Opt. Soc. Am. B **14**, 2268 (1997)
48 L. Becouarn, E. Lallier, M. Brevignon, J. Lehoux: Opt. Lett. **23**, 1508 (1998)
49 L.A. Eyres, P.J. Torreau, T.J. Pinguet, C.B. Ebert, J.S. Harris, M.M. Fejer, L. Becouarn, B. Gerard, E. Lallier: Appl. Phys. Lett. **79**, 904 (2001)
50 A. Szilagyi, A. Horduik, H. Schlossberg: J. Appl. Phys. **47**, 2025 (1976)
51 L. Gordon, G.L. Woods, R.C. Eckardt, R.R. Route, R.S. Feigelson, M.M. Fejer, R.L. Byer: Electron. Lett. **29**, 1942 (1993)
52 G.D. Boyd, C.K.N. Patel: Appl. Phys. Lett. **8**, 313 (1966)
53 H. Komine, W.H.J. Long, J.W. Tully, E.A. Stappaerts: Opt. Lett. **23**, 661 (1998)
54 S.J.B. Yoo, R. Bhat, C. Caneau, M.A. Koza: Appl. Phys. Lett. **66**, 3410 (1995)
55 O. Levi, T.J. Pinguet, L.A. Eyres, L. Scaccabarozzi, M.M. Fejer, J.S.J. Harris, T.J. Kulp, S. Bisson, B. Gerard, L. Becouarn, E. Lallier: *Conf. Lasers Electro-Opt*. (OSA Trends Opt. Photon. (TOPS) Vol. 56) (Optical Society of America, Baltimore, MA 2001)